



## Protein-drug conjugate programmed by pH-reversible linker for tumor hypoxia relief and enhanced cancer combination therapy

Xican Zhang<sup>a</sup>, Liangzhu Feng<sup>b,\*</sup>, Ziliang Dong<sup>b</sup>, Xiaoqian Xin<sup>a</sup>, Zhijuan Yang<sup>b</sup>, Dashi Deng<sup>b</sup>, Ernst Wagner<sup>c</sup>, Zhuang Liu<sup>b</sup>, Xiaowen Liu<sup>a,\*</sup>

<sup>a</sup> Clinical Translational Center for Targeted Drug, Department of Pharmacology, School of Medicine, Jinan University, Guangzhou 510632, Guangdong Province, China

<sup>b</sup> Institute of Functional Nano & Soft Materials (FUNSOM), Jiangsu Key Laboratory for Carbon-Based Functional Materials & Devices, Soochow University, Suzhou 215123, China

<sup>c</sup> Pharmaceutical Biotechnology, Center for System-based Drug Research, Ludwig-Maximilians-Universität München, Butenandtstrasse 5-13, D-81377 Munich, Germany



### ARTICLE INFO

#### Keywords:

Protein-drug  
Cancer  
Combinational therapy  
pH-reversible  
Tumor microenvironment  
Dynamic bond

### ABSTRACT

Combining functional proteins with small molecular drugs into one entity may endow distinct synergistic advantages. However, on account of completely different physicochemical properties of such payloads, co-delivery through systemic administration for therapeutic purpose is challenging. Herein, we designed the protein-drug conjugate HSAP-DC-CAT (human serum albumin/Pt (IV)-dibenzocyclooctyne/chlorin e6-catalase) by modification of CAT and cisplatin pro-drug loaded HSA with pH-sensitive azide linker 3-(azidomethyl)-4-methyl-2,5-furandione (AzMMMan) followed by click chemistry assembly with DC. The dynamic covalent bonds between linker and proteins, on the one hand, can bridge proteins and small molecular drugs in the intermediate state for systemic delivery in the harsh in vivo environment; on the other hand, it can trigger traceless cleavage and release of drugs and proteins with full bioactivity in acidic microenvironment of tumor. The multifunctional HSAP-DC-CAT provides efficient cytosolic transduction in vitro, excellent blood half-lives after systemic administration, and significant antitumor outcome via integrated cisplatin-based chemotherapy and Ce6-based photodynamic therapy enhanced by catalase-induced manipulation of tumor hypoxia microenvironment. This study describes a universal formulation strategy for protein and small molecular drug by a bifunctional linker through amide reaction and click chemistry, with traceless in vivo release of therapeutic units.

### 1. Introduction

Solid tumor microenvironments (TME) impose diverse biological barriers including tumor hypoxia, reduced pH and other hostile features on the effective cancer treatments (Estrella et al., 2013; Maas et al., 2012; Trédan et al., 2007). Several pioneering strategies, enabling efficient TME modulation by smart nanodrug delivery systems (NDDSs) (Jain, 2013; Mura et al., 2013; Torchilin, 2014), have been proposed to benefit these tumor characteristic parameters for better therapeutic specificity and efficiency. Given that the negative role of tumor hypoxia on cancer treatment, it has been shown that catalase and its mimics integrated NDDSs are able to efficiently normalize the TME for hypoxia relief by promoting the decomposition of endogenous H<sub>2</sub>O<sub>2</sub> to generate O<sub>2</sub>, thereby providing a favorable condition for photodynamic therapy (PDT) (Shi et al., 2019) and other oxygen-consuming cancer therapy (Prasad et al., 2014; Song et al., 2016b; Zhang et al., 2017). Meanwhile,

the acidic TME, though negatively impairs most cancer treatments, provides a unique chemical environment for the design of tumor-acidity-responsive NDDSs, enabling significantly enhanced therapeutic specificity and efficacy (Danhier et al., 2010; Du et al., 2018; Liu et al., 2014).

Ascribing to their robust targeting or therapeutic potencies of those proteins and peptides (Carter, 2011; Ibraheem et al., 2014; Lagassé et al., 2017; Leader et al., 2008; Han et al., 2010), protein conjugates have found to be effective biopharmaceuticals with improved selectivity and prolonged blood circulation time, particularly for these PEGylated biotherapeutics (Dozier and Distefano, 2015; Mishra et al., 2016; Turecek et al., 2016). However, considering these PEGylated biotherapeutics are commonly obtained via the irreversible covalent conjugation, their therapeutic effects are often remarkably diminished as the PEG corona would restrict the interaction between these biotherapeutics and their targets (Bailon et al., 2001; Foser et al., 2003; Li

\* Corresponding author.

\*\* Corresponding author.

E-mail addresses: [lzfeng@suda.edu.cn](mailto:lzfeng@suda.edu.cn) (L. Feng), [xwliu231@jnu.edu.cn](mailto:xwliu231@jnu.edu.cn) (X. Liu).

et al., 2016). In addition, combinational therapies of proteins and small molecular drugs would greatly expand the therapeutic potency through realization of synergistic effect between the heterogeneous therapeutics. However, one key dilemma for the optimal therapeutic outcome is the rational formulation of therapeutic protein-drug (Holland et al., 2019), which should protect the proteins from in vivo degradation and denaturation, as well as prolong the circulation time and enhance biocompatibility of small molecular drugs. So far, very few samples have been investigated in this field, and to the best of our knowledge, the reversible covalent binding of therapeutic proteins and small molecular drugs has not been well studied.

To this end, we previously developed azidomethyl-methylmaleic anhydride (AzMMMan) based pH-responsive linker for the reversible PEGylation or conjugation of several different proteins, which showed efficient intracellular delivery and controlled release of proteins with their bioactivity unimpaired (Liu et al., 2016; Liu et al., 2017; Maier and Wagner, 2012). In the present study, we developed the dynamic covalent bond-assisted programmed approach to assemble two small therapeutic drugs with proteins, which could improve the in vivo pharmacokinetics and pharmacodynamics of small molecule drugs and construct a favorable therapeutic microenvironment by proteins for synergistic cancer therapy. For the purpose of decreasing cisplatin associated side effects (Johnstone et al., 2016; Tolan et al., 2016; Wang et al., 2019), the cisplatin(IV)-succinic acid pro-drug (Pt(IV)SA) was conjugated with human serum albumin (HSAP) (Feng et al., 2016). Then AzMMMan was applied as pH-sensitive bifunctional linker to couple with remaining amino groups of HSAP and catalase (CAT) via the pH reversible acyl substitution. In the following, the DBCO coupled photosensitizer Ce6 (Chin et al., 2008; Tan et al., 2016; Tian et al., 2011) was utilized as the cross-linker to initiate the conjugation of these AzMMMan modified proteins (HSAP, CAT) by strain-promoted azide alkyne cycloaddition (SPAAC). The obtained protein-drug of HSAP-DC-CAT showed remarkably enhanced pharmacokinetics and pharmacodynamics of small molecule drugs and well-protected catalytic performance towards H<sub>2</sub>O<sub>2</sub> decomposition. Collectively, HSAP-DC-CAT consisted of four functional units: (i) cisplatin pro-drug (IV) conjugated with HSA to decrease cisplatin associated side effects, for site-directed chemotherapy by conversion into cytotoxic Pt (II) within the intracellular reducing tumor target microenvironment; (ii) small therapeutic drug photosensitizer Ce6 for photodynamic therapy; (iii) CAT, an antioxidant enzyme, to overcome tumor hypoxia by specific catalytic behavior in decomposing H<sub>2</sub>O<sub>2</sub> to produce O<sub>2</sub>, thus providing a favorable TME for the PDT by Ce6; and (iv) the dynamic covalent protein-drug conjugation by an acidic reversible and click reactive bifunctional linker AzMMMan, thus mediating traceless release of unmodified proteins and small molecule drugs at the acidic tumor target microenvironment.

## 2. Materials and methods

### 2.1. Materials

Catalase solution ( $\geq 35,000$  units/mg) was purchased from Aladdin. Chlorin e6 was purchased from J&K Scientific Ltd. Human serum albumin, dimethyl sulfoxide, N-(3-dimethylaminopropyl)-N-ethylcarbodiimide hydrochloride crystalline, N-hydroxysuccinimide, N-hydroxysulfosuccinimide sodium salt and 3-(4,5-dimethylthiazol-2-yl)-2,5-diphenyltetrazolium bromide (MTT) was obtained from Sigma-Aldrich. RPMI-1640 medium and fetal bovine serum were obtained from Thermo Fisher Scientific Inc. All other chemicals were purchased from China National Pharmaceutical Group Corporation and used directly without any further purification.

### 2.2. Characterization and methods

UV-VIS-NIR absorbance spectra were recorded by the Perkin Elmer

Lambda 750 UV-VIS-NIR spectrophotometer. Transmission electron microscopy (TEM) was used to characterize the morphology of HSAP-DC-CAT nanoparticles. The hydrodynamic diameters of conjugates (HSAP-DC-CAT, HSA-DC-CAT, HSAP-DC-HSA and mixture CAT/Ce6/HSAP) with or without acidic buffer incubation were determined by a Zetasizer Nano-ZS (Malvern Instruments, UK). The conjugation assessment of click chemistry (HSAP-DC-CAT, HSA-DC-CAT and HSAP-DC-HSA) and traceless release behavior of conjugates (HSAP-DC-CAT) treated with acidic buffer was determined by SDS-polyacrylamide gel electrophoresis (SDS-PAGE) or Zetasizer Nano-ZS.

The portable dissolved oxygen meter was used to detect the O<sub>2</sub> production treated by free catalase and HSAP-DC-CAT with different concentrations of H<sub>2</sub>O<sub>2</sub>, by recording the dissolved oxygen concentration continuously.

The method of detecting singlet oxygen was reported previously (Chen et al., 2017; Li et al., 2013). In simply, singlet oxygen sensor green reagent (SOSG, molecular probes) was dissolved in methanol firstly and added to the prepared samples ([SOSG] = 2.5  $\mu$ M, [Ce6] = 1  $\mu$ M). Then samples were irradiated by 660 nm light at 5 mW/cm<sup>2</sup> in nitrogen atmosphere. The measurement of SO generation was determined by SOSG fluorescence signals at 530 nm with excitation at 494 nm.

The catalase activity of HSAP-DC-CAT was determined by the Góth method (Góth, 1991). Briefly, 0.5 mL hydrogen peroxide (50 mM) was added to free catalase or HSAP-DC-CAT solution and incubated for 1 min at 37 °C. Then the reaction was terminated by adding 0.5 mL ammonium molybdate (32.4 mM) by forming stable yellow complexes with the residual H<sub>2</sub>O<sub>2</sub>. After cooling down to 25 °C, the absorbance of each sample was measured at 400 nm by the UV-VIS-NIR spectrometer to determine catalase activity. The relative activity of catalase was calculated by the following equation: relative catalytic activity = (absorbance of H<sub>2</sub>O<sub>2</sub> with PBS – absorbance of H<sub>2</sub>O<sub>2</sub> with HSAP-DC-CAT) / (absorbance of H<sub>2</sub>O<sub>2</sub> with PBS – absorbance of H<sub>2</sub>O<sub>2</sub> with free CAT). To measure the stability of catalase against protease digestion, both free catalase and HSAP-DC-CAT were incubated with protease K (0.5 mg/ml) at 37 °C. At different time points, the catalase activity of samples was measured by aforementioned Góth method.

### 2.3. Synthesis of 3-(azidomethyl)-4-methyl-2,5-furandione (AzMMMan)

The BrMMMan intermediate was synthesized by using a previous protocol (Liu et al., 2016; Maier and Wagner, 2012). In brief, dimethylmaleic anhydride (5.04 g, 40 mmol), N-bromosuccinimide (14.24 g, 80 mmol), and benzoyl peroxide (0.2 g, 0.83 mmol) were added into an adaptive round-bottom flask and dissolved in carbon tetrachloride (CCl<sub>4</sub>, 250 mL). The reaction was stirred for 5 h under refluxing. Then the mixture was cooled down to room temperature, benzoyl peroxide (0.2 g, 0.83 mmol) was added as catalyst to the mixture again, the reaction was stirred for another 5 h under refluxing. Then the mixture was again cooled down to room temperature, and solids were removed by filtration. The obtained solution was washed two times with DI water (100 mL) and one time with saturated sodium chloride solution by separating funnel, then the organic solution dried over anhydrous sodium sulfite for 3 h and concentrated to a thick yellow oil by rotary evaporator. The crude intermediate was purified by chromatography on a silica gel column (elution with petroleum ether/ethyl acetate 4:1). Finally, BrMMMan intermediate (purity 96%, 1.1 g) was obtained (Fig. S2a). BrMMMan: <sup>1</sup>H NMR (500 MHz, CDCl<sub>3</sub>)  $\delta$  (ppm) = 2.18 (s, 3H, –CH<sub>3</sub>), 4.18 (s, 2H, –CH<sub>2</sub>-Br), 7.26 (CHCl<sub>3</sub>).

The AzMMMan was similarly synthesized as previously reported (Liu et al., 2016; Maier and Wagner, 2012). Briefly, BrMMMan (1.5 mmol), sodium azide (1.6 mmol) and dry acetone (15 mL) were added into a 50 mL round-bottom flask. The reaction was stirred for 12 h under room temperature. The crude product was obtained by filtering and evaporating. After that, the final product was purified by silica gel column (eluent, hexane/ethyl acetate = 7:3). AzMMMan

(95.5 mg) was obtained after evaporating the eluent (Fig. S2b). AzMMMan:  $^1\text{H NMR}$  (500 MHz,  $\text{CDCl}_3$ ),  $\delta$  (ppm) = 2.23 (s, 3H,  $-\text{CH}_3$ ), 4.29 (s, 2H,  $-\text{CH}_2-\text{N}_3$ ), 7.26 ( $\text{CHCl}_3$ ).

#### 2.4. Synthesis of DBCO-Ce6

DBCO-PEG<sub>4</sub>-CH<sub>2</sub>CH<sub>2</sub>NH<sub>2</sub> in this experiment was used to introduce DBCO groups onto Ce6 by the reaction of amino groups with carboxyl groups of Ce6. In brief, Ce6 (1 eq) was pre-dispersed in DMSO and activated by EDC (5 eq) and NHS (5 eq) for 1 h. Then DBCO-PEG<sub>4</sub>-CH<sub>2</sub>CH<sub>2</sub>-NH<sub>2</sub> (2.5 eq) and TEA (5 eq) were added into the solution and the mixture was reacted for 12 h, resulting in DBCO-Ce6.

#### 2.5. Modification of proteins with AzMMMan

AzMMMan was used to reversibly introduce azide groups into catalase, or serum albumin (HSA) by the reaction of excessive maleic anhydride group from AzMMMan with amino groups of the proteins. Briefly, AzMMMan (10 mg) dissolved in 50  $\mu\text{L}$  acetonitrile was slowly added into catalase solution (10 mg) in Hepes buffer pH 9.0 and reacted for 4 h. CAT-AZ was obtained after ultrafiltration by a centrifugal filter device (molecular weight cut-off, MWCO = 10 kDa) to remove excessive free AzMMMan.

Succinic acid-derivatized cisplatin prodrug (Pt (IV)SA) was prepared by oxidation and acidification of cisplatin according to a previous protocol (Feng et al., 2016). HSA (10 mg, 1 eq) reacted with Pt (IV)SA (0.653 mg, 10 eq) which was first activated by EDC and NHS in DMSO for 0.5 h. The mixture was stirred for 12 h in PBS (pH 8.0) in the dark. HSA-Pt (IV) was obtained after centrifugation at 4500 rpm for 5 min to remove possible precipitate and ultrafiltration by a centrifugal filter device (molecular weight cut-off, MWCO = 10 kDa) to remove free small molecules. Pt (IV)-HSA-AZ was then prepared analogously as described for CAT-AZ.

#### 2.6. Synthesis of protein-drug conjugates by click chemistry

HSAP-DC-CAT conjugates were prepared by the click chemistry reaction of DBCO-Ce6 with azide groups of AzMMMan-modified proteins (Fig. S3). In brief, DBCO-Ce6 (1 eq to 1 eq AzMMMan from proteins-AZ) was used to bridge CAT-AZ (5 mg) and Pt (IV)-HSA-AZ (5 mg) in PBS (pH 8.0), the mixture reacted for 6 h, then the resulting protein conjugates were PEGylated.

As a control, HSAP-DC-HSA were prepared by the similar procedure by replacement of CAT with HSA as described in the synthesis of HSAP-DC-CAT. HSA-DC-CAT without cisplatin was also prepared analogously except that no Pt (IV)SA was previously introduced onto HSA (Fig. S3, Fig. S4). Furthermore, the CAT/Ce6/HSAP mixture as another control was obtained by simply physical mixing of CAT, Ce6 and HSAP.

The drug loading rate of these conjugates were calculated by using the following equations: Ce6 loading rate = determined Ce6 content in conjugate/initial Ce6 content for DBCO-Ce6 conjugation; Pt loading rate = determined Pt content in conjugate/initial Pt content for conjugation with HSA (Table S1).

#### 2.7. pH-responsive release of proteins

HSAP-DC-CAT, HSA-DC-CAT, HSAP-DC-HSA and mixture CAT/Ce6/HSAP were incubated in PBS buffer (pH 7.4, pH 6.0) for 8 h, and the hydrodynamic diameters of these treated conjugates were determined by dynamic light scattering (DLS) (Fig. S5). Additionally, the protein release from various conjugates in different acidic conditions was evaluated by SDS-PAGE (Fig. S6).

#### 2.8. Cell experiment

Murine breast cancer cells (4T1) were obtained from American Type

Culture Collection (ATCC) and cultured in RPMI-1640 medium including 10% fetal bovine serum (FBS) and 1% penicillin/streptomycin at 37 °C, 5% CO<sub>2</sub>.

To study the cellular internalization efficiency of HSAP-DC-CAT and free Ce6, 4T1 cells were seeded into 12 well plates and then incubated with HSAP-DC-CAT and free Ce6 (Ce6, 10  $\mu\text{M}$ ) for 4 h. Confocal imaging and flow cytometry were carried out to study the internalization of HSAP-DC-CAT and control group.

To detect the reactive oxygen species (ROS) in vitro, 4T1 cells were incubated with free Ce6, HSAP-DC-HSA and HSAP-DC-CAT separately. DCFH-DA was used as fluorescence probe. The ROS level in these groups were confirmed by confocal imaging.

For studying the chemotherapy effect when treated with HSAP-DC-CAT or free cisplatin, 4T1 cells in 96-well plates were incubated with different concentrations of free cisplatin or HSAP-DC-CAT for 24 h. The standard MTT assay was used for measuring the cell relative viabilities.

For combinational therapy of PDT and chemotherapy, 4T1 cells were seeded into 96-well plates and then incubated with various concentrations of free Ce6 and HSAP-DC-CAT. After 4 h incubation, samples were incubated for 30 min with or without irradiation by 660 nm light at 5 mW/cm<sup>2</sup>. After 24 h of additional incubation, MTT assay was used for determining the relative viabilities of cells.

For enhanced combinational therapy of PDT and chemotherapy, 4T1 cells were firstly seeded into 96-well plates and cultured in a hypoxic cell incubator (5% CO<sub>2</sub>, 94% N<sub>2</sub>, 1% O<sub>2</sub>) for 24 h, and subsequently incubated with different concentrations of HSAP-DC-CAT and free Ce6 for 4 h. Then these samples were irradiated by 660 nm light at 5 mW/cm<sup>2</sup> for 30 min with or without adding 100  $\mu\text{M}$  H<sub>2</sub>O<sub>2</sub> in advance. After that, samples were transferred into normal condition and incubated for 24 h with fresh media. MTT assay was carried out to measure the cell viabilities after various treatments.

In order to find out whether HSAP-DC-CAT in the acidic environment would enhance their deep penetration, multicellular tumor spheroids (MCTS) were used as model system, to evaluate migration ability of HSAP-DC-CAT in different pH conditions. In briefly, MCTS were firstly incubated with HSAP-DC-CAT at pH 6.5 or 7.4 for 24 h and then washed with normal PBS. Then, MCTS were fixed by 4% formaldehyde and dehydrated by sugar solutions for frozen section. The MCTS slices were stained with DAPI for confocal imaging to determine the migration of HSAP-DC-CAT (Fig. S7).

#### 2.9. Animal experiment

To establish the animal model, female nude mice were purchased from Nanjing Peng Sheng Biological Technology Co Ltd. All animal experiments were performed according to the guidelines for the protection of animal life and were approved by Laboratory Animal Ethics Committee in Soochow University. For tumor inoculation, 4T1 cells (about  $2 \times 10^6$ ) were suspended in 50  $\mu\text{L}$  PBS and finally injected subcutaneously into the back of mice.

For in vivo imaging and distribution studies, HSAP-DC-CAT or CAT/Ce6/HSAP (Ce6, 0.5 mg/ml, 200  $\mu\text{L}$ ) was intravenously injected into mice (Ce6 dose: 5 mg/kg). Blood was drawn from tail vein of mice at different time points after intravenous injection. The mice were then sacrificed, organs including liver, spleen, kidneys, heart, lung and tumor were obtained and used for ex vivo imaging by a Maestro in vivo optical imaging system.

For in vivo combinational therapy, nude mice with 4T1 tumors ( $\sim 100 \text{ mm}^3$ ) were divided into five groups: (1) Untreated; (2) i.v. injected with HSAP-DC-CAT and irradiated with 660 nm light at 4 h p.i.; (3) i.v. injected with HSAP-DC-CAT without irradiation; (4) i.v. injected with HSAP-DC-HSA and irradiated by 660 nm light at 4 h p.i.; (5) i.v. injected with HSA-DC-CAT and irradiated by 660 nm light at 4 h p.i. The dose of Ce6 and cisplatin were kept at 5 mg/kg and 85  $\mu\text{g}/\text{kg}$ , respectively. The weight of mice of different groups were recorded (Fig. S8), lengths and widths of tumor measured with a digital caliper were

recorded every two days for 2 weeks. The tumor volume was calculated by the formula:  $\text{width}^2 \times \text{length} / 2$ .

The histological properties of tumors with various treatment were analyzed by hematoxylin and eosin (H&E) staining assay. The H&E staining tumor slices were collected. The damaged stated of various tumors were then assessed by confocal imaging.

### 3. Results and discussion

In the few recent decades, protein-based therapeutics including their drug conjugates presented a great opportunity for treatment of a variety of human diseases, owing to high specificity and high potency derived from their amino-acid-based secondary and tertiary structure (Chen et al., 2017; Song et al., 2016a; Song et al., 2016b). However, the interaction force between proteins and formulation counterpart should be rational balanced. The interaction should be strong enough to withstand the in vivo hostile environment. In additional, the interaction should not influence the bioactivity of protein therapeutics and drugs, result in reducing the therapeutic outcome. For example, PEGylated interferon- $\alpha$ 2a, as FDA approved in 2001 for treating hepatitis, retains only 10% activity of unmodified interferon- $\alpha$ 2a (Bailon et al., 2001; Foser et al., 2003).

#### 3.1. Dynamic covalent bond-assisted protein-drug formulation HSAP-DC-CAT

Protein-drug conjugates present promising biopharmaceuticals for clinical usage. Nonetheless, the conjugation of proteins to their drug counterparts should be rationally designed to avoid inactivation of their functional activities (Chen et al., 2017; Leader et al., 2008; Song et al., 2016a). To circumvent this possible pitfall, we explored our previous developed tumor acidity responsive bifunctional AzMMMan (Liu et al., 2016; Liu et al., 2017; Maier and Wagner, 2012) as the dynamic covalent linker for the fabrication of a multifunctional protein-drug conjugate for effective cancer treatment. For this purpose, we chose CAT as a therapeutic protein model, pro-drug Pt (IV) and Ce6 as small molecule drugs to study this novel type of protein-drug conjugate (Fig. 1, Fig. S1). In briefly, the pro-drug Pt (IV)-COOH was firstly conjugated with parts of amino groups of HSA and free pro-drug Pt (IV) was removed by ultrafiltration, the anchored Pt (IV) was quantified by inductively coupled plasma mass spectrometry (ICP-MS). In the following, CAT and Pt (IV) loaded HSA were then coupled with excess acidic reversible bifunctional linker AzMMMan (Fig. S2) by the reaction of maleic anhydride groups with amino groups of the proteins. After that, the HSAP-DC-CAT were obtained through a crosslinking process by click chemistry of DBCO coupled Ce6 (DC) with AzMMMan modified proteins by strain-promoted azide alkyne cycloaddition. The resulting protein conjugates were PEGylated. Besides of this, HSAP-DC-HSA conjugates without CAT, HSA-DC-CAT conjugates without pro-drug Pt (IV) and CAT/Ce6/HSAP mixture without AzMMMan were also prepared by similar covalent reaction or simple physical mixing for the following control experiments.

The conjugates were then analyzed by SDS-PAGE to confirm the successful assembly (Fig. S3). Compared to the unmodified CAT, HSA and CAT/Ce6/HSA mixture, the SDS-PAGE gel revealed the shortest migration for HSAP-DC-CAT, HSAP-DC-HSA and HSA-DC-CAT conjugates, which could be explained by the successful click conjugation of DC with AzMMMan modified HSAP, HSA and CAT. The loading contents of Pt (IV) and Ce6 of HSAP-DC-CAT conjugates were 74.2% and 73.2% respectively determined by ICP-MS and UV-VIS-NIR spectra (Table S1).

As revealed by the UV-VIS-NIR absorption spectra of CAT, CAT-AZ, HSA, Pt(IV)-HSA-AZ, Ce6 and HSAP-DC-CAT, HSAP-DC-CAT showed a new absorption band around 664 nm compared to CAT and CAT-AZ (Fig. 2a), which derived from the interaction of photosensitizer Ce6 with HSA. Interestingly, compared with the absorption peak of free Ce6

(~652 nm), the red shift in HSAP-DC-CAT was observed, likely a result from the covalent bonding between Ce6 and HSAP or CAT (Chen et al., 2017). Meanwhile, HSAP-DC-CAT exhibited two new absorption bands at 402 nm and 504 nm compared to HSA, indicated the successful conjugation of CAT (Fig. 2a). The fabricated HSAP-DC-CAT showed uniform size with average diameter around ~120–200 nm as revealed by transmission electron microscopy (TEM) imaging (Fig. 2b), collaboratively demonstrated by the hydrodynamic diameters of 164 nm measured with DLS (Fig. 2c). In addition, HSA-DC-CAT and HSAP-DC-HSA showed again the increased size compared to CAT/Ce6/HSA mixture (Fig. S4), in corresponding to the SDS-PAGE results in Fig. S3, as result of the click conjugation. All these complementary analyses verified the successful conjugation of CAT-AZ, Pt (IV)-HSA-AZ with DBCO modified Ce6 by click chemistry.

#### 3.2. Acidic pH reversibility

The AzMMMan linker offers the opportunity for acidic pH-reversible modifications of proteins (Liu et al., 2016; Liu et al., 2017; Maier and Wagner, 2012). To evaluate the acidic sensitivity of HSAP-DC-CAT, HSAP-DC-CAT was incubated at different pH conditions (pH 7.4, 6.5). The DLS measurement together with TEM observation showed a reduction of size of HSAP-DC-CAT from 164 nm to 21 nm when incubated in acidic pH 6.5 buffer (Fig. 2d), collaboratively demonstrated by the size shrinking of HSA-DC-CAT, HSAP-DC-HSA and HSAP-DC-HSA (Fig. S5). Meanwhile, HSAP-DC-CAT treated with normal buffer (pH 7.4) did not show obvious alteration of size. This indicates that the HSAP-DC-CAT conjugate formulation could be dissociated under acidic environment. The conjugates without or with treatment in acidic buffer were also analyzed by SDS-PAGE to confirm successful conjugation and dynamic release under acidic conditions (Fig. S3, Fig. S6). The SDS-PAGE gel of HSAP-DC-CAT showed a lower shift distance compared to the unmodified HSA and CAT, which demonstrates successful assembly of proteins with DC, as also revealed by aforementioned TEM and DLS measurement. Meanwhile, the HSAP-DC-CAT treated with acidic buffers displayed a similar migration compared to that of HSA and CAT, verifying again that the covalent binding of HSA-AZ, CAT-AZ with DC could be cleavage triggered in acidic environment (Fig. 2d, Fig. S5, Fig. S6).

Inspired by the pH-dissociation of HSAP-DC-CAT conjugates, which might be beneficial for cancer therapy along with the shrink size of the conjugates in the acidic TME, their penetration into the solid tumor was investigated. The multicellular tumor spheroids (MCTS) model of solid tumor was incubated with HSAP-DC-CAT conjugates at different pH conditions (pH 7.4, pH 6.5). The fluorescence of MCTS treated with HSAP-DC-CAT at pH 6.5 was stronger than treatment at pH 7.4, as revealed by confocal imaging (Fig. S7). This indicates a better intratumoral penetration in the acidic microenvironment as a result of the dynamic formulation strategy.

#### 3.3. Enzyme activity assessment

Catalase, one of the highest catalytic efficiency enzyme in organs to decompose  $\text{H}_2\text{O}_2$  to  $\text{H}_2\text{O}$  and  $\text{O}_2$ , has been investigated to adjust the hypoxia condition in the TME (Song et al., 2016a). To demonstrate that the HSAP-DC-CAT would also catalyze the decomposition of  $\text{H}_2\text{O}_2$ , an abundant metabolite in the tumor tissue, to  $\text{H}_2\text{O}$  and  $\text{O}_2$ , the catalytic performance of HSAP-DC-CAT and control groups were rationally studied by a portable dissolved oxygen probe. Compared to the unmodified CAT, the cross-linked HSAP-DC-CAT also performed high catalytic activity of decomposition of  $\text{H}_2\text{O}_2$  to generate  $\text{O}_2$  in 2 min. (Fig. 3a), though with a reduced efficiency which could be explained by the partial inhibition of the enzyme after conjugation, but this expected to be restored when the enzyme traceless cleavage release in acidic environment. As expected, the catalytic ability of  $\text{H}_2\text{O}_2$  to  $\text{O}_2$  by HSAP-DC-CAT is a concentration dependent process (Fig. 3a). However, in the

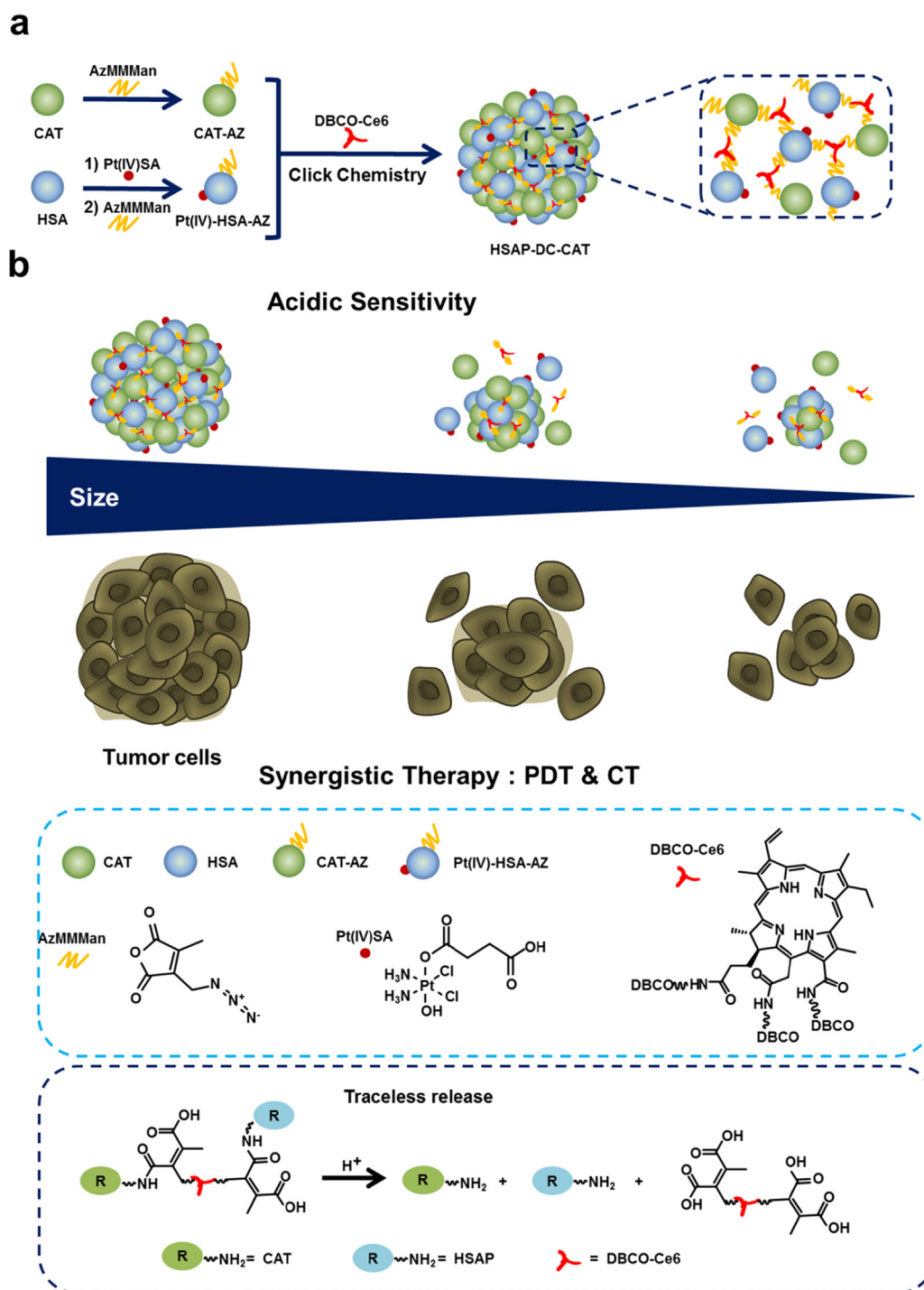


**Fig. 1.** A scheme illustrating the synthesis process of HSAP-DC-CAT and traceless pH-responsive release of payloads. (a) HSAP-DC-CAT were fabricated by click chemistry of DBCO-Ce6 with AzMMMan modified HSA and CAT. (b) Schematic description of diminishing solid tumor by accumulated HSAP-DC-CAT and degradation of HSAP-DC-CAT triggered by acidic tumor microenvironment.

absence of catalase-containing group, a negligible  $O_2$  was detected which indicated  $H_2O_2$  solution was rather stable at the experimental condition (Fig. 3a).

Motivated by the highly efficient generation of  $O_2$  catalysis by HSAP-DC-CAT, the generation of singlet oxygen (SO) was then studied, which would be greatly beneficial for PDT in a tumor hypoxia microenvironment. The concentration of SO was measured by the singlet oxygen sensor green (SOSG) probe (Chen et al., 2017), when HSAP-DC-CAT treated with or without 0.5 mM  $H_2O_2$ , which was to mimic the metabolic TME. It is noteworthy that high SO generation was detected

when treated HSAP-DC-CAT together with  $H_2O_2$ , owing to the efficient production of  $O_2$  by catalytic decomposition of  $H_2O_2$ . Meanwhile, the generation of SO treated only with HSAP-DC-CAT or free  $H_2O_2$  was much lower than that of treated with both reagents (Fig. 3b). This simulation experiment of TME could indirectly prove that the HSAP-DC-CAT would reconstruct a beneficial therapeutic parameter of abundant SO for the following PDT.

Though the activity of CAT from HSAP-DC-CAT to decompose  $H_2O_2$  would be partially inhibited compared to unmodified CAT, but this could be beneficial in vivo physiological environment, as unmodified

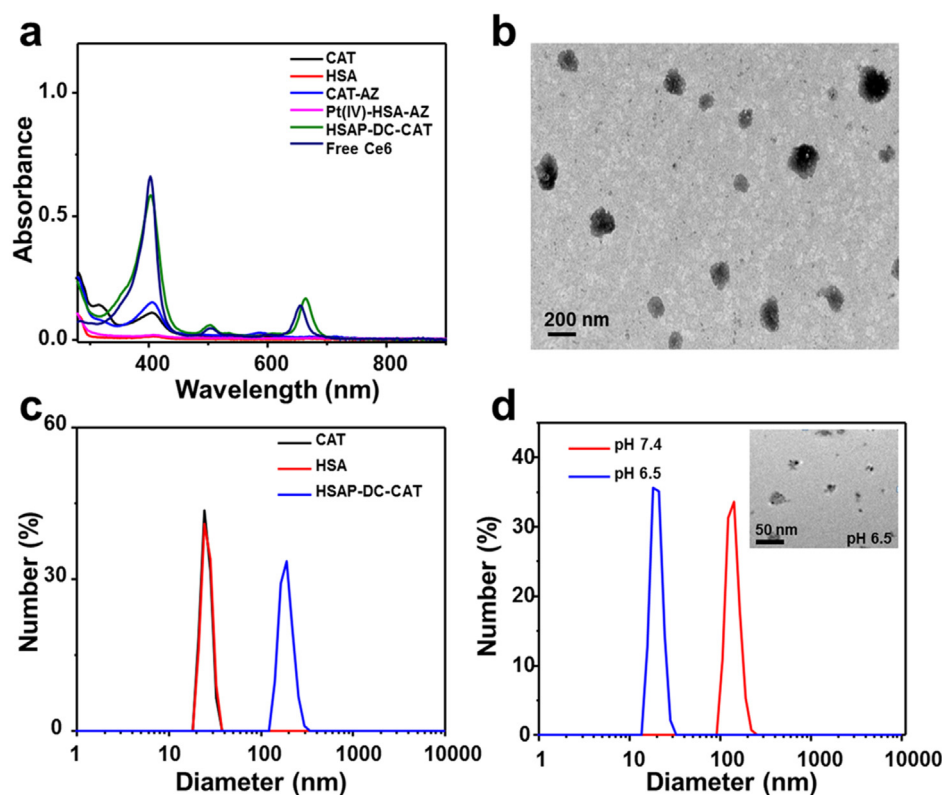


**Fig. 2.** Characterization of HSAP-DC-CAT. (a) UV-vis-NIR spectra of free CAT, HSA, Ce6, CAT-AZ, Pt(IV)-HSA-AZ and HSAP-DC-CAT. (b) TEM imaging of HSAP-DC-CAT in buffer (pH 7.4). (c) DLS measurement of free CAT, HSA and HSAP-DC-CAT in buffer (pH 7.4). (d) DLS measurement of HSAP-DC-CAT in different pH conditions (pH 7.4, 6.5) and TEM imaging of HSAP-DC-CAT treated in pH 6.5 buffer.

CAT was exposed to a hostile environment in the presence of proteases, which would result in the frequent deactivation of unmodified CAT. To determine whether the conjugation would be beneficial for the protection of CAT bioactivity, HSAP-DC-CAT and free CAT were treated with proteases, and activities of CAT from both were investigated by the Góth method (Góth, 1991). Compared to the unmodified CAT, most of which lost its bioactivity in 24 h during treatment with protease K (0.5 mg/ml), CAT from HSAP-DC-CAT conjugates could maintain most enzyme bioactivity (69.5%) ever after 24 h when incubated with the same concentration of protease K applied for unmodified CAT (Fig. 3c). This might offer an optimal protection strategy of the CAT for its targeting delivery to TME, as well as for other therapeutic proteins which perform their functions *in vivo*.

### 3.4. Intracellular delivery and cytotoxicity

After the characterization of HSAP-DC-CAT, their cellular internalization and *in vitro* cytotoxicity was investigated. HSAP-DC-CAT was efficiently internalized into 4T1 cells, as indicated by the confocal laser

scanning microscopy (CLSM) (Fig. 4a) and flow cytometry (Fig. 4b), thus providing the internalized Pt (IV) as anchored in HSAP-DC-CAT the proper location to perform its therapeutic cancer cell killing effect. Consequently, cell viability assays (MTT) were performed with various concentration (Pt: 0.625  $\mu$ M, 1.25  $\mu$ M, 2.5  $\mu$ M, 5  $\mu$ M) of HSAP-DC-CAT and free cisplatin quantified by ICP-MS to investigate the biological activity and effect on 4T1 cell viability after 24 h incubation. Both HSAP-DC-CAT and free cisplatin showed a cytotoxicity towards to 4T1 cancer cells which was concentration dependent, with HSAP-DC-CAT at 5  $\mu$ M presenting most efficient cell killing ability (Fig. 4c).

In the following we wanted to evaluate whether the conjugated CAT from HSAP-DC-CAT could improve the intracellular concentration of reactive oxygen species (ROS), which would be expected to enhance the therapeutic effect for PDT. The intracellular generation of ROS by adding ROS detector DCFH-DA was imaged after incubation with Ce6, HSAP-DC-HSA and HSAP-DC-CAT conjugates. It was found that generation of ROS was much higher when treated with HSAP-DC-CAT conjugates than that of Ce6 and HSAP-DC-HSA treatment without CAT (Fig. 4d), as revealed by the green signal only observed from HSAP-DC-

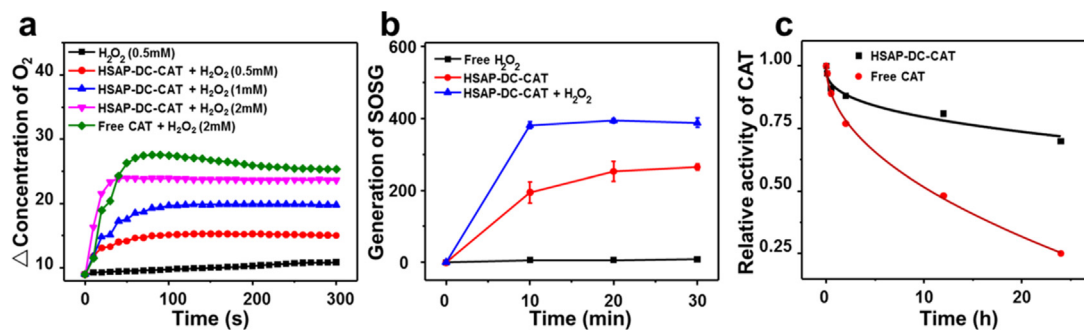


**Fig. 3.** Enzyme activity assessment. (a) Oxygen generation treated with free CAT or HSAP-DC-CAT in the presence of various  $H_2O_2$  concentrations. (b) The generation of singlet oxygen determined by the increased SOSG fluorescence for free  $H_2O_2$  and HSAP-DC-CAT with or without adding  $H_2O_2$ . (c) Relative bioactivity of free CAT and HSAP-DC-CAT after treatment with proteinase K assay.

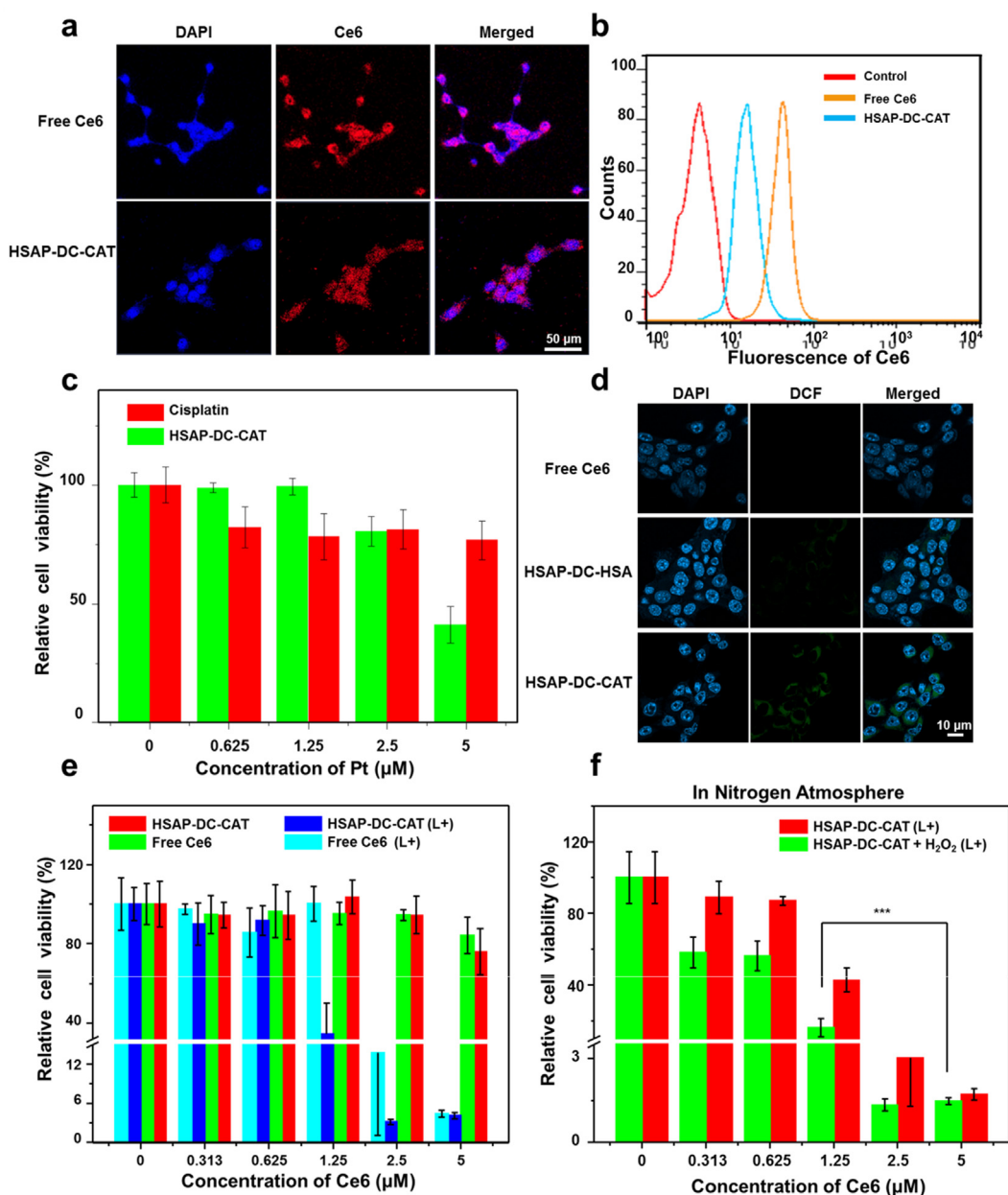


**Fig. 4.** Intracellular delivery and cytotoxicity. (a) Confocal fluorescence images of 4T1 cells after incubation with free Ce6 and HSAP-DC-CAT. Blue and red colors represented DAPI-stained cell nuclei and Ce6 fluorescence respectively. (b) Flow cytometry of 4T1 cells after incubation with free Ce6 and HSAP-DC-CAT. (c) Relative cell viability of 4T1 treated with cisplatin and HSAP-DC-CAT at different Pt concentrations. (d) Reactive oxygen species (ROS) in 4T1 cells were imaged by the confocal laser scanning microscope (CLSM) by adding DCFH-DA, after incubation with free Ce6, HSAP-DC-HSA and HSAP-DC-CAT. (e) Relative cell viability of 4T1 treated with free Ce6 and HSAP-DC-CAT with or without irradiation at a various concentrations of Ce6. (f) Relative cell viability of 4T1 treated with HSAP-DC-CAT with or without adding  $H_2O_2$  in the presence of different Ce6 concentrations under irradiation. P values were calculated by Student's *t*-test (\*\*\*)  $p < 0.001$ . (For interpretation of the references to colour in this figure legend, the reader is referred to the web version of this article.)

#### CAT group.

Having demonstrated that HSAP-DC-CAT assisted ROS generation, the 4T1 cancer cell viability was evaluated by MTT after treated with HSAP-DC-CAT conjugates at various concentrations without or with light irradiation. Compared to the treatment with Ce6 or HSAP-DC-CAT without light irradiation, the combinational treatment by HSAP-DC-CAT under NIR irradiation showed the highest cell killing ability towards to 4T1 cancer cells, as revealed only 3.1% cells viability when treated at the 2.5  $\mu M$  conjugated Ce6 (Fig. 4e), which is much more effective than previously reported (Chen et al., 2017). It has to be mentioned that HSAP-DC-CAT presumably display a higher cytotoxicity than cells treated with Ce6 under NIR irradiation, due to the extra synergistic therapeutic effect from Pt (IV), as also explained in the above-

mentioned paragraph.

Furthermore, considering that CAT could help to decompose endogenous  $H_2O_2$  within the TME to produce oxygen, we also checked whether the therapeutic outcome would be further improved with exogenous  $H_2O_2$  to mimic TME under nitrogen atmosphere. The cell cytotoxicity of HSAP-DC-CAT treatment in the presence of  $H_2O_2$  (for enhanced ROS generation) under NIR irradiation showed encouraging therapeutic effects; cancer cells viability treated with 2.5  $\mu M$  (quantified by Ce6) HSAP-DC-CAT in the presence of  $H_2O_2$  under NIR irradiation was only 1.3%, far lower than that treatment without  $H_2O_2$  incubation (Fig. 4f), as a result of enhanced PDT improved by the generation of ROS by catalytic degradation of  $H_2O_2$  with CAT. To the best of our knowledge, this is the lowest concentration of Ce6 for potent

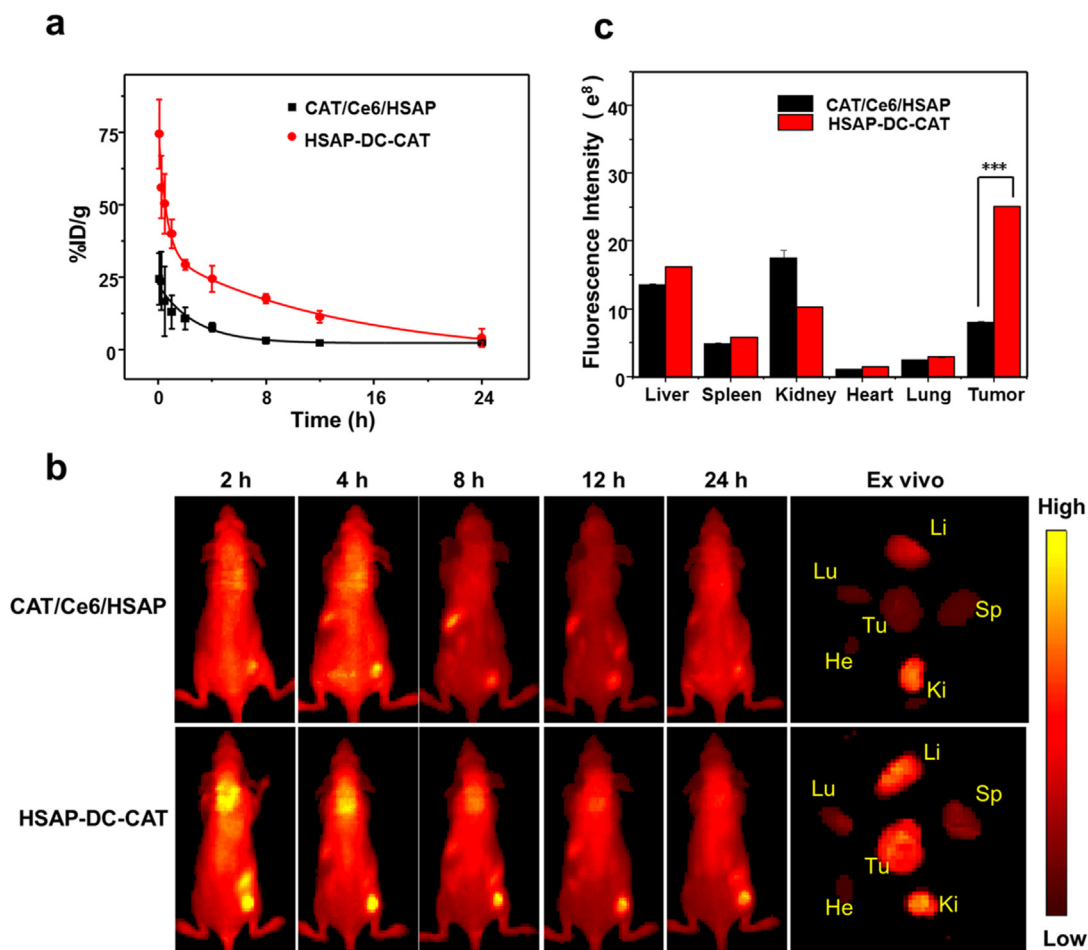


**Fig. 5.** In vivo pharmacokinetic behaviors of HSAP-DC-CAT. (a) The blood circulation of CAT/Ce6/HSAP mixture and HSAP-DC-CAT conjugates after tail intravenous injection (3 mice each group). (b) In vivo fluorescence imaging of 4T1 tumor-bearing mice with intravenous injection of CAT/Ce6/HSAP and HSAP-DC-CAT at different time points, and ex vivo fluorescence images of major organs at 24 h post injection. Li, Sp, Ki, He, Lu and Tu stand for liver, spleen, kidney, heart, lung and tumor, respectively. (c) Quantification of ex vivo fluorescence images for those organs (24 h p.i) from b). P values were calculated by Student's t-test (\*\*\*)  $p < 0.001$ .

cancer cell killing. In sum, HSAP-DC-CAT showed an excellent cancer cell killing ability in a synergistic setting of a programmed drug formulation strategy.

### 3.5. In vivo pharmacokinetics and pharmacodynamics

Considering that the remarkable in vitro cancer cells killing ability by treatment with HSAP-DC-CAT, the in vivo pharmacokinetics and pharmacodynamics of HSAP-DC-CAT were then investigated. Herein, the simple physical mixture of CAT, Ce6 and HSAP (CAT/Ce6/HSAP) was carried out as the control experiment, to verify whether the dynamic covalent bondage of fabricated HSAP-DC-CAT would enhance their in vivo behavior and therapeutic efficacy. Mice were intravenously injected with the dynamic covalent bond conjugate HSAP-DC-CAT and the control mixture CAT/Ce6/HSAP at the same dose of Ce6 (5 mg/kg). The in vivo behavior of conjugates and control mixture was tracked at different time points post injection based on the fluorescence of Ce6. As detected by the fluorescence of Ce6 in the extracted blood at various time, the blood circulation half-lives of HSAP-DC-CAT was calculated and found to be much longer than that of CAT/Ce6/HSAP mixture (8.05 h compared to 2.74 h, Fig. 5a). HSAP-DC-CAT apparently were sufficiently stable in the blood circulation environment, with the covalent binding between components to resist the hostile environment in the blood. On the contrary, the simple physical mixture of CAT/Ce6/HSAP by intermolecular forces, which are much weaker than covalent bonding, might be easily dissociated in the blood,

resulting in inferior blood circulation.

After confirming suitable in vivo circulation of HSAP-DC-CAT, mice bearing subcutaneous 4T1 tumors were imaged by a Maestro EX in vivo imaging system at different time points post injection of HSAP-DC-CAT or the CAT/Ce6/HSAP mixture. The fluorescence of Ce6 from both HSAP-DC-CAT and mixture CAT/Ce6/HSAP were diffuse within the whole body of mouse at the early time points (Fig. 5b). Subsequently, the mouse showed excellent tumor accumulation with injected HSAP-DC-CAT, as visible by the strong fluorescence of Ce6 at tumor tissue even at 24 h post-injection, whereas much weaker fluorescent signals were observed at the tumor of mice injected with CAT/Ce6/HSAP (Fig. 5b). The semi-quantitative analysis of fluorescence distribution through various tissues and organs confirmed that mice treated with HSAP-DC-CAT performed much higher tumor accumulation (40.6–16.8%) for potential therapeutics (Fig. 5c), while mice treated with CAT/Ce6/HSAP mixture showed higher accumulation in kidney. The superior tumor accumulation of HSAP-DC-CAT might be contributed by the covalent binding strategies for the protein-drug formulation, as also discussed in the previous section.

Motivated by the excellent blood circulation half-lives and superior tumor accumulation of the HSAP-DC-CAT, their combination therapy at different conditions was performed in vivo with the 4T1 tumor model (Fig. 6a). To investigate the therapeutic outcome by treatment with HSA-DC-CAT or other control groups, the mice were divided into five groups (five mice for one group): untreated, HSAP-DC-CAT without irradiation, HSA-DC-CAT (Ce6, 5 mg/kg) with 660 nm light for 1 h,

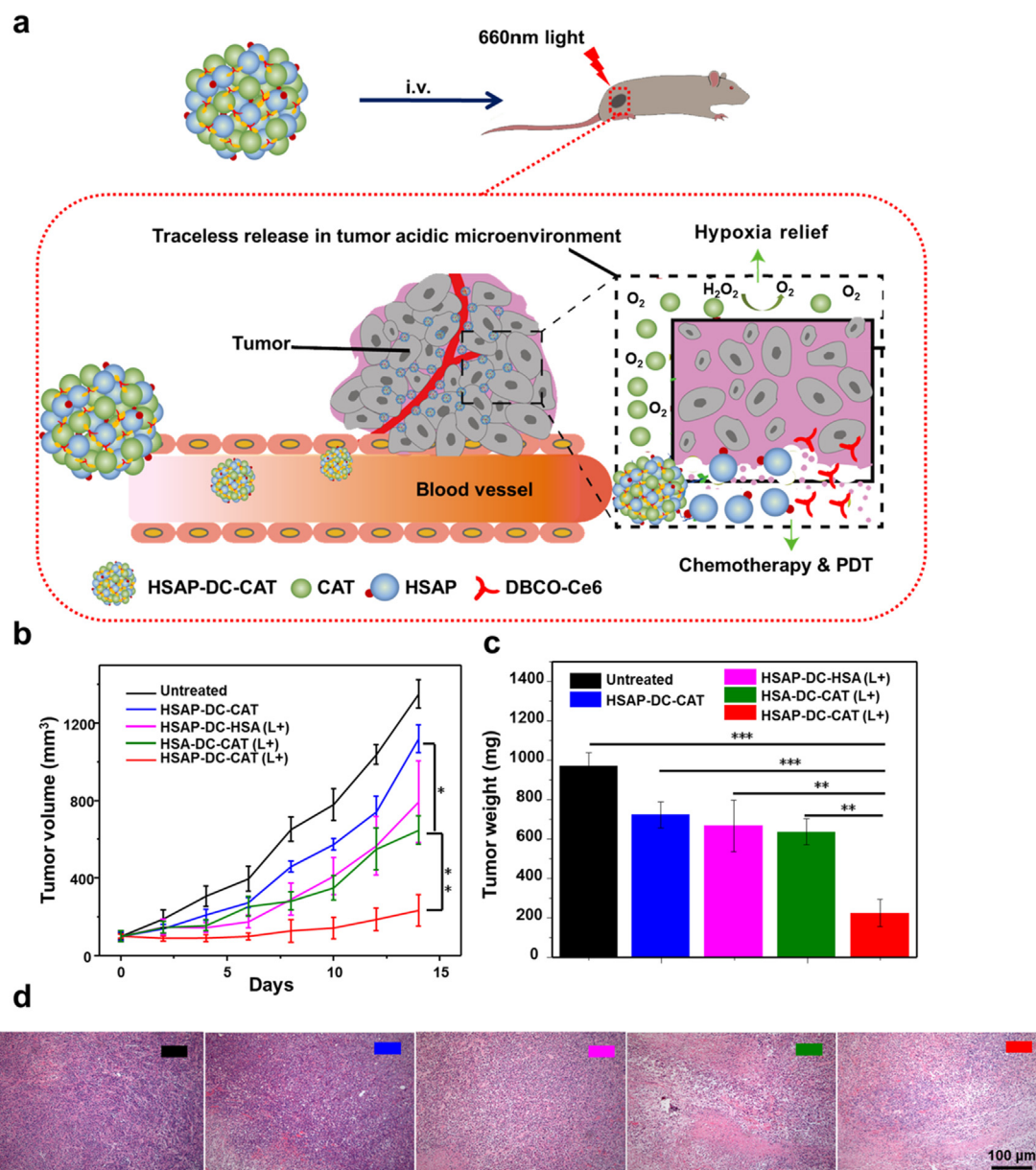


**Fig. 6.** In vivo combination therapy. (a) Scheme of HSAP-DC-CAT behavior in TME. (b) Tumor growth curves of mice ( $n = 5$  per group) in different treatment groups (i.v. injection). Untreated; HSAP-DC-CAT irradiated at 660 nm light at 4 h post-injection (p.i.); HSAP-DC-CAT without irradiation; HSAP-DC-HSA irradiated at 660 nm light at 4 h p.i.; HSA-DC-CAT irradiated at 660 nm light at 4 h p.i.; (c) Average tumor weight after various treatments. P values were calculated by Student's  $t$ -test: \* $p < 0.1$ , \*\* $p < 0.01$ , \*\*\* $p < 0.001$  ( $n = 5$ ). (d) H&E stained tumor slices from different groups collected 24 h p.i (scale bars: 100  $\mu\text{m}$ ).

HSAP-DC-HSA (Ce6, 5 mg/kg; Pt, 85  $\mu\text{g}/\text{kg}$ ) with 660 nm light for 1 h, HSAP-DC-CAT (Ce6, 5 mg/kg; Pt, 85  $\mu\text{g}/\text{kg}$ ) with 660 nm light for 1 h. After various treatments, the tumor size was monitored every two days for two weeks with a caliper (Fig. 6b). The therapeutic outcome was most encouraging; the mice treated with HSAP-DC-CAT under NIR irradiation showed best antitumor effects among the various treatment groups, presumably due to the combination effects of PDT with Ce6, Pt for chemotherapeutic activity, CAT to improve the ROS generation for enhanced PDT (Fig. 6a), acidic cleavage of DC for deeper intratumoral penetration of therapeutics (Fig. S7). The HSA-DC-CAT group without Pt chemotherapeutic activity, the HSAP-DC-CAT group without NIR irradiation for PDT, the HSAP-DC-HSA group without CAT to improve ROS generation, all showed lesser therapeutic effects compared to the optimal protein-drug conjugate formulation HSAP-DC-CAT (Fig. 6b).

The therapeutic outcome was also evaluated by the tumor weight of various treatments. It again revealed that the HSAP-DC-CAT group with 660 nm light had the most effective therapeutic effect with smallest

tumors (225 mg weight) compared to other control groups (heavier than 600 mg) (Fig. 6c). Meanwhile, none of the treatments with the different protein-drug formulation showed obvious cytotoxicity, as the weight of mice maintained normal physical state during treatments (Fig. S8). Furthermore, the histology analysis of tumor slices collected after various treatments was performed by hematoxylin and eosin (H&E) staining (Fig. 6d). The most efficient tumor cell destruction was observed for the treatment by HSAP-DC-CAT with 660 nm light, while other control groups, for example HSAP-DC-HSA (pink line) without CAT to improve ROS generation, had reduced or negligible damaged cancer cells. Overall, our study demonstrated the high efficiency of tumor inhibition by dynamic covalent bond conjugate formulation of the combination protein-drug conjugate HSAP-DC-CAT.

#### 4. Conclusion

In this study, a balanced protein-drug conjugate HSAP-DC-CAT with

an acidic-reversible bifunctional linker (AzMMMan) by amidation and click chemistry has been first developed. The conjugated HSAP-DC-CAT integrated small molecular drugs for chemotherapy (Pt pro-drug) and enhanced PDT (Ce6) with an enzyme (CAT) for hypoxia normalization of TME. The covalent binding of proteins and drugs would benefit both for favorable in vivo circulation and control release of payloads for better therapeutic outcome. Pharmacokinetic studies showed the prolonged circulation half-lives of dynamic covalent conjugated HSAP-DC-CAT (8.05 h), as compared to the physical mixture of CAT/Ce6/HSAP (2.74 h), demonstrating the advantages of conjugation. Meanwhile, the HSAP-DC-CAT conjugates accumulated in the tumor tissue could bring about synergistic effect by small molecular drugs Ce6, pro-drug Pt (IV) with therapeutic protein to improve the hypoxia microenvironment of tumor. Given that abundant amino groups on proteins, we expect the pH-labile trace-less conjugation method should be applicable for many therapeutic proteins with reactive small molecular drugs.

### CRedit authorship contribution statement

**Xican Zhang:** Investigation, Formal analysis, Data curation. **Liangzhu Feng:** Conceptualization, Methodology, Project administration, Supervision, Writing - review & editing. **Ziliang Dong:** Methodology, Data curation. **Xiaoqian Xina:** Methodology, Data curation. **Zhijuan Yang:** Methodology, Data curation. **Dashi Deng:** Methodology, Data curation. **Ernst Wagner:** Writing - review & editing. **Zhuang Liu:** Project administration, Supervision. **Xiaowen Liu:** Project administration, Funding acquisition, Conceptualization, Methodology, Supervision, Writing - original draft, Writing - review & editing.

### Declaration of Competing Interest

The authors declare that they have no known competing financial interests or personal relationships that could have appeared to influence the work reported in this paper.

### Acknowledgements

This work was supported by the startup funding from Jinan University and Jiangsu Key Laboratory for Carbon-Based Functional Materials & Devices, Soochow University, and the Fundamental Research Funds for the Central Universities (No. 11618337), National Natural Science Foundation of China (No. 81903546).

### Appendix A. Supplementary material

Supplementary data to this article can be found online at <https://doi.org/10.1016/j.ijpharm.2020.119321>.

### References

- Bailon, P., Palleroni, A., Schaffer, C.A., Spence, C.L., Fung, W.-J., Porter, J.E., Ehrlich, G.K., Pan, W., Xu, Z.-X., Modi, M.W., Farid, A., Berthold, W., Graves, M., 2001. Rational design of a potent, long-lasting form of interferon: a 40 kDa branched polyethylene glycol-conjugated interferon  $\alpha$ -2a for the treatment of hepatitis C. *Bioconjugate Chem.* 12, 195–202.
- Carter, P.J., 2011. Introduction to current and future protein therapeutics: A protein engineering perspective. *Exp. Cell Res.* 317, 1261–1269.
- Chen, Q., Chen, J., Liang, C., Feng, L., Dong, Z., Song, X., Song, G., Liu, Z., 2017. Drug-induced co-assembly of albumin/catalase as smart nano-theranostics for deep intra-tumoral penetration, hypoxia relieve, and synergistic combination therapy. *J. Control. Release* 263, 79–89.
- Chin, W.W.L., Heng, P.W.S., Thong, P.S.P., Bhuvaneshwari, R., Hirt, W., Kuenzel, S., Soo, K.C., Olivo, M., 2008. Improved formulation of photosensitizer chlorin e6 polyvinylpyrrolidone for fluorescence diagnostic imaging and photodynamic therapy of human cancer. *Eur. J. Pharm. Biopharm.* 69, 1083–1093.
- Ibraheem, D., Elaissari, A., Fessi, H., 2014. Administration strategies for proteins and peptides. *In. J. Pharm.* 477, 578–589.
- Danhier, F., Feron, O., Pr at, V., 2010. To exploit the tumor microenvironment: passive and active tumor targeting of nanocarriers for anti-cancer drug delivery. *J. Control. Release* 148, 135–146.
- Dozier, J.K., Distefano, M.D., 2015. Site-specific PEGylation of therapeutic proteins. *Int. J. Mol. Sci.* 16, 25831–25864.

- Du, J., Li, H., Wang, J., 2018. Tumor-Acidity-Cleavable Maleic Acid Amide (TACMAA): a powerful tool for designing smart nanoparticles to overcome delivery barriers in cancer nanomedicine. *Acc. Chem. Res.* 51, 2848–2856.
- Estrella, V., Chen, T., Lloyd, M., Wojtkowiak, J., Cornnell, H.H., Ibrahim-Hashim, A., Bailey, K., Balagurunathan, Y., Rothberg, J.M., Sloane, B.F., Johnson, J., Gatenby, R.A., Gillies, R.J., 2013. Acidity generated by the tumor microenvironment drives local invasion. *Cancer Res.* 73, 1524–1535.
- Feng, L., Gao, M., Tao, D., Chen, Q., Wang, H., Dong, Z., Chen, M., Liu, Z., 2016. Cisplatin-prodrug-constructed liposomes as a versatile theranostic nanoplatform for bimodal imaging guided combination cancer therapy. *Adv. Funct. Mater.* 26, 2207–2217.
- Foser, S., Schacher, A., Weyer, K.A., Brugger, D., Dietel, E., Marti, S., Schreitm uller, T., 2003. Isolation, structural characterization, and antiviral activity of positional isomers of monopegylated interferon  $\alpha$ -2a (PEGASYS). *Protein Expres. Purif.* 30, 78–87.
- Han, L., Huang, R., Liu, S., Huang, S., Jiang, C., 2010. Peptide-conjugated PAMAM for targeted doxorubicin delivery to transferrin receptor overexpressed tumors. *Mol. Pharm.* 7, 2156–2165.
- Holland, J.P., Gut, M., Klingler, S., Fay, R., Guillo, A., 2019. Photochemical reactions in the synthesis of protein-drug conjugates. *Chem. Eur. J.* 26, 33–48.
- Jain, R.K., 2013. Normalizing tumor microenvironment to treat cancer: bench to bedside to biomarkers. *J. Clin. Oncol.* 31, 2205–2218.
- Johnstone, T.C., Suntharalingam, K., Lippard, S.J., 2016. The next generation of platinum drugs: targeted Pt(II) agents, nanoparticle delivery, and Pt(IV) prodrugs. *Chem. Rev.* 116, 3436–3486.
- G oth, L., 1991. A simple method for determination of serum catalase activity and revision of reference range. *Clin. Chim. Acta* 196, 143–151.
- Lagass e, H., Alexaki, A., Simhadri, V., Katagiri, N., Jankowski, W., Sauna, Z., Kimchi-Sarfaty, C., 2017. Recent advances in (therapeutic protein) drug development [version 1; peer review: 2 approved]. *F1000Research* 6.
- Leader, B., Baca, Q.J., Golan, D.E., 2008. Protein therapeutics: a summary and pharmacological classification. *Nat. Rev. Drug Discov.* 7, 21–39.
- Li, Y., Lin, J., Liu, G., Ma, J., Xie, L., Guo, F., Zhu, X., Hou, Z., 2016. Dual-acting, function-responsive, and high drug payload nanospheres for combining simplicity and efficacy in both self-targeted multi-drug co-delivery and synergistic anticancer effect. *Int. J. Pharm.* 512, 194–203.
- Li, Z., Wang, C., Cheng, L., Gong, H., Yin, S., Gong, Q., Li, Y., Liu, Z., 2013. PEG-functionalized iron oxide nanoclusters loaded with chlorin e6 for targeted, NIR light induced, photodynamic therapy. *Biomaterials* 34, 9160–9170.
- Liu, J., Huang, Y., Kumar, A., Tan, A., Jin, S., Mozhi, A., Liang, X., 2014. pH-sensitive nano-systems for drug delivery in cancer therapy. *Biotechnol. Adv.* 32, 693–710.
- Liu, X., Zhang, P., He, D., R odl, W., Prei , T., R adler, J.O., Wagner, E., L achelt, U., 2016. pH-reversible cationic RNase A conjugates for enhanced cellular delivery and tumor cell killing. *Biomacromolecules* 17, 173–182.
- Liu, X., Zhang, P., R odl, W., Maier, K., L achelt, U., Wagner, E., 2017. Toward artificial immunotoxins: traceless reversible conjugation of RNase A with receptor targeting and endosomal escape domains. *Mol. Pharm.* 14, 1439–1449.
- Maas, A.L., Carter, S.L., Wileyto, E.P., Miller, J., Yuan, M., Yu, G., Durham, A.C., Busch, T.M., 2012. Tumor vascular microenvironment determines responsiveness to photodynamic therapy. *Cancer Res.* 72, 2079–2088.
- Maier, K., Wagner, E., 2012. Acid-labile traceless click linker for protein transduction. *J. Am. Chem. Soc.* 134, 10169–10173.
- Mishra, P., Nayak, B., Dey, R.K., 2016. PEGylation in anti-cancer therapy: An overview. *Asian J. Pharm. Sci.* 11, 337–348.
- Mura, S., Nicolas, J., Couvreur, P., 2013. Stimuli-responsive nanocarriers for drug delivery. *Nat. Mater.* 12, 991–1003.
- Prasad, P., Gordijo, C.R., Abbasi, A.Z., Maeda, A., Ip, A., Rauth, A.M., DaCosta, R.S., Wu, X.Y., 2014. Multifunctional albumin-MnO<sub>2</sub> nanoparticles modulate solid tumor microenvironment by attenuating hypoxia, acidosis, vascular endothelial growth factor and enhance radiation response. *ACS nano* 8, 3202–3212.
- Shi, J., Wang, T., You, Y., Luqman, A.M., Liu, Z., Han, F., Li, Y., Wang, Y., 2019. Enhancement of ultralow-intensity NIR light-triggered photodynamic therapy based on exo- and endogenous synergistic effects through combined glutathione-depletion chemotherapy. *Nanoscale* 11, 13078–13088.
- Song, G., Chen, Y., Liang, C., Yi, X., Liu, J., Sun, X., Shen, S., Yang, K., Liu, Z., 2016a. Catalase-loaded TaOx nanoshells as bio-nanoreactors combining high-Z element and enzyme delivery for enhancing radiotherapy. *Adv. Mater.* 28, 7143–7148.
- Song, X., Feng, L., Liang, C., Yang, K., Liu, Z., 2016b. Ultrasound triggered tumor oxygenation with oxygen-shuttle nanoporous carbon to overcome hypoxia-associated resistance in cancer therapies. *Nano Lett.* 16, 6145–6153.
- Tan, X., Pang, X., Lei, M., Ma, M., Guo, F., Wang, J., Yu, M., Tan, F., Li, N., 2016. An efficient dual-loaded multifunctional nanocarrier for combined photothermal and photodynamic therapy based on copper sulfide and chlorin e6. *Int. J. Pharm.* 503, 220–228.
- Tian, B., Wang, C., Zhang, S., Feng, L., Liu, Z., 2011. Photothermally enhanced photodynamic therapy delivered by nano-graphene oxide. *ACS Nano* 5, 7000–7009.
- Tolan, D., Gandin, V., Morrison, L., El-Nahas, A., Marzano, C., Montagner, D., Erxleben, A., 2016. Oxidative stress induced by Pt(IV) pro-drugs based on the cisplatin scaffold and indole carboxylic acids in axial position. *Sci. Rep.* 6, 29367.
- Torchilin, V.P., 2014. Multifunctional, stimuli-sensitive nanoparticulate systems for drug delivery. *Nat. Rev. Drug Discov.* 13, 813–827.
- Tr edan, O., Galmarini, C.M., Patel, K., Tannock, I.F., 2007. Drug resistance and the solid tumor microenvironment. *J. Natl. Cancer Inst.* 99, 1441–1454.
- Turecek, P.L., Bossard, M.J., Schoetens, F., Ivens, I.A., 2016. PEGylation of biopharmaceuticals: a review of chemistry and nonclinical safety information of approved drugs. *J. Pharm. Sci.* 105, 460–475.
- Wang, Z., Deng, Z., Zhu, G., 2019. Emerging platinum(IV) prodrugs to combat cisplatin resistance: from isolated cancer cells to tumor microenvironment. *Dalton T.* 48, 2536–2544.
- Zhang, R., Song, X., Liang, C., Yi, X., Song, G., Chao, Y., Yang, Y., Yang, K., Feng, L., Liu, Z., 2017. Catalase-loaded cisplatin-prodrug-constructed liposomes to overcome tumor hypoxia for enhanced chemo-radiotherapy of cancer. *Biomaterials* 138, 13–21.